Excitation of Ultraslow High-q Surface Plasmon Polariton Modes in Dense Arrays of Double-Walled Carbon Nanotubes

Alexey S. Kadochkin,* Sergey G. Moiseev, Vyacheslav V. Svetukhin, Alexander N. Saurov, and Igor O. Zolotovskii

This work explores the plasmonic properties of parallel double-walled carbon nanotube arrays. It is shown that ultraslow surface plasmon polariton (SPP) modes possessing a phase velocity some orders of magnitude lower than the speed of light in vacuum and high *Q*-factor can be generated in such arrays. It is demonstrated that nonrelativistic electron beams with the velocity less than 10^6 m s^{-1} can be used to excite SPPs in arrays of double-walled carbon nanotubes. For the SPP modes excited by an electron beam, the frequency range of SPP waves and electron beam velocities corresponding to the phase matching within a wide frequency range are determined. It opens the way to design slow-wave structures based on the dense arrays of multiwalled carbon nanotubes employing an efficient energy transfer from the pump to the SPPs.

1. Introduction

Due to high demand in THz sources for spectroscopic and medical applications, elaboration of THz generators has become one of the most rapidly growing fields.[1–3] Arrays of parallel carbon nanotubes (CNTs) and nanocomposites based on them are being enthusiastically studied as promising tool for generation and handling of electromagnetic radiation in various frequency ranges, from optical to microwave.[4–12] CNT arrays are effectively exploited for fabrication of radiation absorbers,[6,9] sensors,[13] thermal emitters,[4,10] signal processing devices,[5,11] terahertz, and IR emitters.[12]

A. S. Kadochkin, S. G. Moiseev, I. O. Zolotovskii
Ulyanovsk State University
Ulyanovsk, Russian Federation
E-mail: a_kadochkin@inbox.ru

A. S. Kadochkin, S. G. Moiseev, A. N. Saurov, I. O. Zolotovskii
Institute of Nanotechnologies of Microelectronics of the Russian Academy of Sciences
Moscow, Russian Federation

S. G. Moiseev
Kotelnikov Institute of Radio Engineering and Electronics of the Russian Academy of Sciences
Ulyanovsk Branch, Ulyanovsk, Russian Federation

V. V. Svetukhin
Scientific-Manufacturing Complex "Technological Centre"
Moscow 124498, Russian Federation

Recently, it has been shown that CNTs can be considered as a plasmonic waveguide enabling propagation of an ultraslow surface electromagnetic wave (with the effective refractive index > 100) in the THz range.[14,15] Such ultraslow modes cannot be excited in CNT by an external electromagnetic wave using standard optical schemes due to a high effective refractive index of ultraslow waves propagating in CNTs. However, they could be generated and amplified through the injection of electron beams propagating along the parallel CNTs.[16] For an effective interaction between the electromagnetic radiation and injected current, the phase matching between the amplified wave and carrier velocity has to be provided. The interaction mechanism, in this case, is similar to that in a traveling wave tube.[17,18] One-dimensional nature of CNT used as a waveguide limits the phase space for charge carriers, thus strongly reducing the scattering and increasing mobility of the carriers,[19] enables phase matching due to high charge carrier velocity.

Diverse fabrication technologies have been elaborated for arrays of single-[4,5] and multiwalled[6–8] CNTs (SWCNTs and MWCNTs respectively) with controllable parameters. Commonly, the fabricated CNT arrays (unless special efforts are made[20]) are multiwalled[21,22] and the chirality cannot be set to their layers in advance and often is unknown. To date, the plasmonic properties of the MWCNT have not been widely discussed in the literature. There are only a few studies (see, e.g., ref. [23]) offering rather a sophisticated theory hardly applicable to predict the plasmonic properties of MWCNT arrays in practices. In the present work, the plasmonic properties of dense MWCNT arrays are explored and a simple electromagnetic model of CNT array taking into account their main structural properties is proposed.

2. MWCNT Conductivity Model

A key issue in the study of MWCNT plasmonic properties is elaboration of the model able to describe their conductivity. Various models, in particular, the effective medium model,[6] ab initio models[14,23] taking into account, to different extent, an effect of the CNT array structural properties on their conductivity have been proposed to describe MWCNT properties. The structure of MWCNTs has been thoroughly studied by the X-ray diffraction methods. MWCNTs are thought as hollow or solid cylinders

**ADVANCED
SCIENCE NEWS**

www.advancedsciencenews.com

annalen
der **physik**

www.ann-phys.org

with the diameters ranging from some nanometers to some tens of nanometers with the layers spaced by the distance of 0.3–0.4 nm.[20–22] Within the layer, there is a strong covalent bonding between carbon atoms, whereas atomic interaction between the layers is due to the weaker van der Waals forces[24] slightly affecting the electron shells and band structure of individual graphene layers composing a MWCNT.[25] The interlayer conductivity of MWCNTs is explored experimentally[26,27]. It has been shown that the static conductivity along the layers is much higher than the interlayer conductivity.[26] An effect of CNT structural properties, in particular, chirality on the plasmonic properties of single-walled CNTs has been studied using the random phase approximation method.[25,28] It has been shown that the plasmonic properties of doped CNT are determined mainly by the concentration of free carriers and by some definite doping level are almost independent of chirality and CNT conductivity type (semiconductor or metal) determined by the band structure.[25,28] Besides, the curvature of CNT walls (rolled graphene layer) has almost no effect on the band structure in CNTs with a diameter much larger than 1 nm.[25,28] Thus, to simulate the plasmonic properties of doped (CNT doping methods are widely represented in the literature, see for example[29,30]) CNTs with a large diameter the conductivity calculated for graphene can be used[31–33]:

$$\sigma(\omega) = \sigma^{inter}(\omega) + \sigma^{intra}(\omega)$$

$$\sigma^{intra}(\omega) = \frac{2ie^2 k_B T}{\pi \hbar^2 (\omega + i\tau^{-1})} \ln\left[2\cosh\left(\frac{\mu}{2k_B T}\right)\right]$$

$$\sigma^{inter}(\omega) = \frac{e^2}{4\pi\hbar}\left[\frac{\pi}{2} + \arctan\left(\frac{\hbar\omega - 2\mu}{2k_B T}\right)\right.$$

$$\left. - \frac{i}{2}\ln\frac{(\hbar\omega + 2\mu)^2}{(\hbar\omega - 2\mu)^2 + (2k_B T)^2}\right] \quad (1)$$

In Equation (1), σ^{inter} and σ^{inter} are the contribution of inter- and intraband transitions, e is the electron charge, $\hbar$ is the Planck constant, k_B is the Boltzmann constant, T is the temperature, μ is the graphene chemical potential, τ is the average lifetime of carriers. For numerical calculations, the following parameters are taken: $T = 300$ K, $\mu = 0.2$ eV, and $2\pi\hbar/\tau = 0.1$ meV.[34] The used value of chemical potential of doped graphene corresponds to the surface concentration of carriers $n = 1.2 \ 10^{13}$ cM^{-2}[31] and corresponds to one extra charge carrier per thousand carbon atoms.

At the frequencies of some tens of THz, the intraband term σ^{intra} dominates in Equation (1). At low temperatures, when $\mu \gg kT$[31] (it is the case for the used μ and T), Equation (1) is reduced to the well-known Drude-like formula widely used for characterization of CNT conductivity in THz range[35]:

$$\sigma^{intra} = \frac{ie^2 |\mu|}{\pi\hbar^2 (\omega + i\tau^{-1})} \quad (2)$$

Therefore, to study the plasmonic properties of doped MWCNT with a diameter of about 10 nm, it is reasonable to assume a CNT as a set of infinitesimally thin layers independently placed one into another with the layer conductivity determined by Equation (1). A more detailed discussion of this issue will be published elsewhere.

3. SPP Dispersion Dependences in Double-Walled Carbon Nanotubes (DWCNTs)

The dispersion dependences of surface plasmon waves have been studied in MWCNT arrays (**Figure 1**) using the conductivity model described by Equation (1). In terms of the model used, MWCNTs are complex waveguides formed as a set of conducting surfaces. Due to variety of surface plasmon modes in MWCNTs, their analysis is fairly difficult. Therefore, we will restrict our attention to double-walled carbon nanotubes (DWCNTs) as the simplest MWCNTs exhibiting the main features of interaction between MWCNTs and electromagnetic radiation.

To plot the dispersion curves for surface plasmon polariton (SPP) we use the modal analysis performed with the COMSOL Multiphysics software. To perform modal analysis we have used 2D model with periodic boundary conditions in x and y directions proposed in[36] (inset in Figure 1). Using this model one can solve the eigenvalue problem for the given geometry and boundary conditions, i.e., to find the complex mode propagation constant $\beta = \beta' - i\beta''$ (here, β' is the SPP propagation constant, β'' is the attenuation constant) for a given frequency ω. **Figure 2**a shows the real and imaginary parts of the SPP complex propagation constant β as the functions of frequency. Negative values of β'' correspond to the SPP attenuation during the propagation along the DWCNT axis. DWCNT arrays are modeled using the periodic boundary conditions for each unit cell as shown in Figure 1.

The cross-sections of plasmon modes in arrays of single- and double-walled CNTs are given in Figure 2b. The dispersive dependences of surface waves propagating in a single SWCNT have been highlighted in our previous studies.[15,36] One can see that in a SWCNT the mode field is concentrated near the surface exhibiting an exponential decrease with the distance from its walls in radial direction (Figure 2b, inset 1). DWCNT also supports propagation of the similar modes with the field concentrated near the outer layer and mainly outside the layer (Figure 2b, inset 2). The dispersion curves describing such mode are given in Figure 2a by the black dash-dotted (β') and dashed (β'') curves. Such SWCNT-like modes can provide the SPP effective refractive index (deceleration coefficient) of about 100 and a high attenuation coefficient of about 10^8 m^{-1} in a wide frequency range. The observed high attenuation coefficient in such modes is due to effective interaction of wide exponential mode "tails" with the conducting walls of neighboring CNTs in the array. As a result, the SPP attenuation coefficient in the array of such CNTs is one or two orders of magnitude higher in absolute value than in a single CNT. One can see (Figure 2a) that in such modes the Q-factor determined as

$$Q = \left|\frac{\beta'}{\beta''}\right| \quad (3)$$

is as small as ≈ 1. These features make such modes unsuitable for applications in slow-wave systems.

The most interesting specific features of the DWCNT modes are associated with the presence of interlayer SPP modes enabling a strong confinement of the field between the layers (Figure 2b, inset 3) and thus providing a high deceleration coefficient at a relatively low absorption coefficient ($|\beta''| \sim 10^6$ m^{-1})
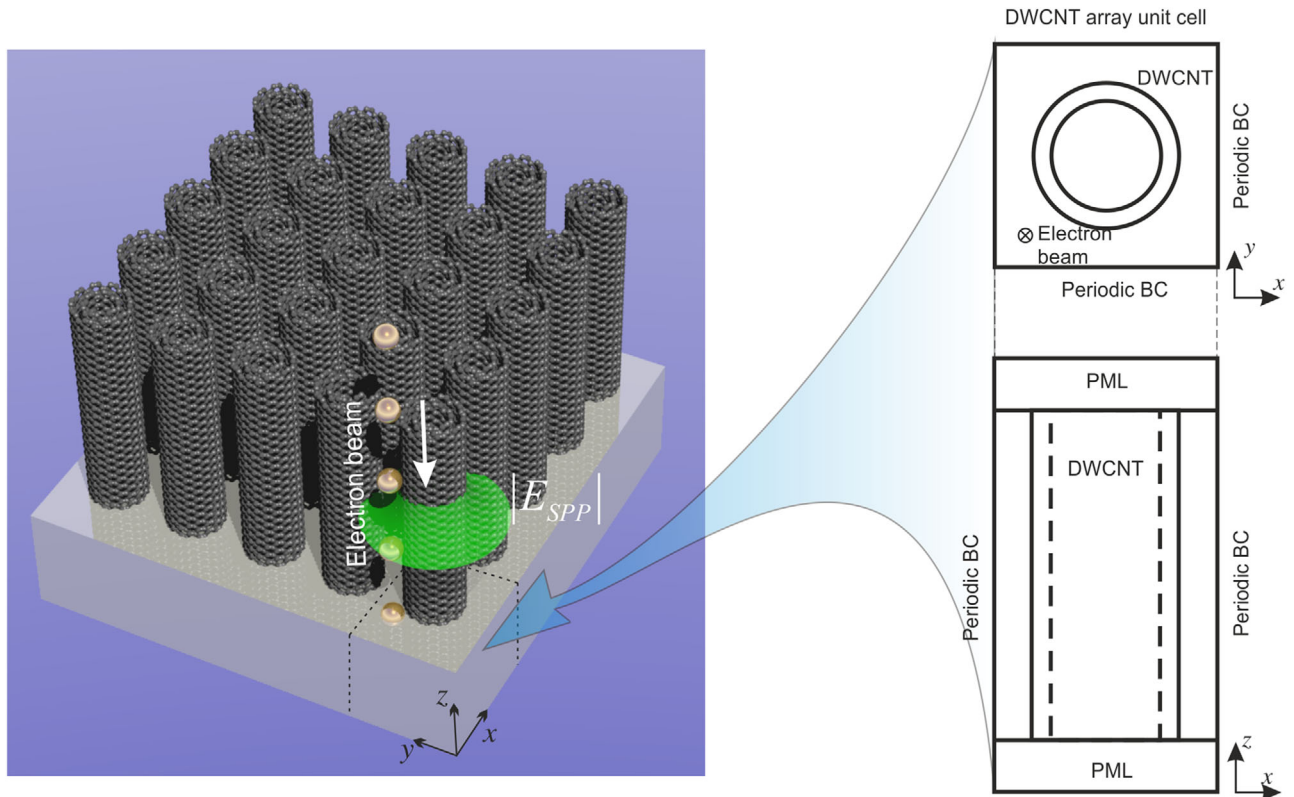
**ADVANCED
SCIENCE NEWS**

www.advancedsciencenews.com

annalen
der **physik**

www.ann-phys.org

Figure 1. Schematic of DWCNT array: nanotubes in the array are irradiated by an electron beam. DWCNT parameters: outer diameter $d = 10$ nm, interlayer distance = 0.34 nm, array constant = 3d. The refractive index of a substrate is equal to one in numerical calculations. Electron beam should be periodically repeated due to periodic boundary conditions in xy-plane but is schematically shown only at one carbon nanotube (CNT) of the array.
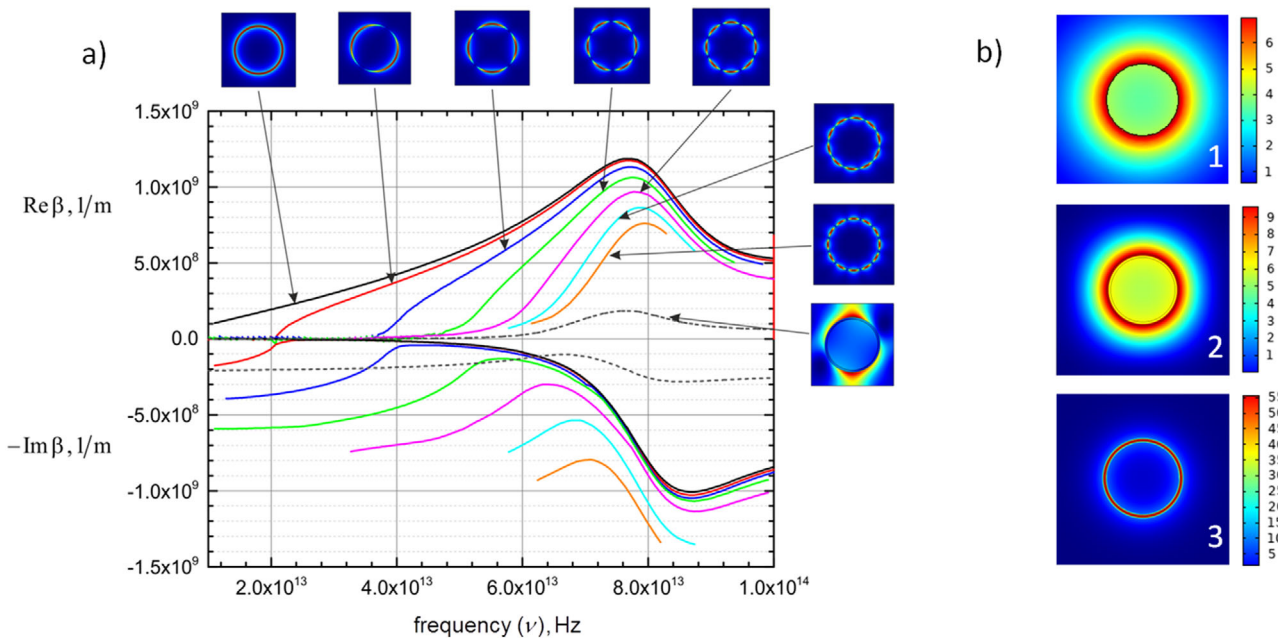

Figure 2. a) Dispersion curves for SPPs propagating in double-walled carbon nanotubes (CNTs; insets are the absolute value of electric field strength over the CNT cross-section for different SPP modes. b) The absolute value of electric field strength (in a.u.) of the azimuthally symmetric surface wave: (1) single-walled CNT (frequency 75 THz), (2) double-walled CNT (frequency 75 THz), and (3) double-walled CNT, interlayer mode (frequency 100 THz).
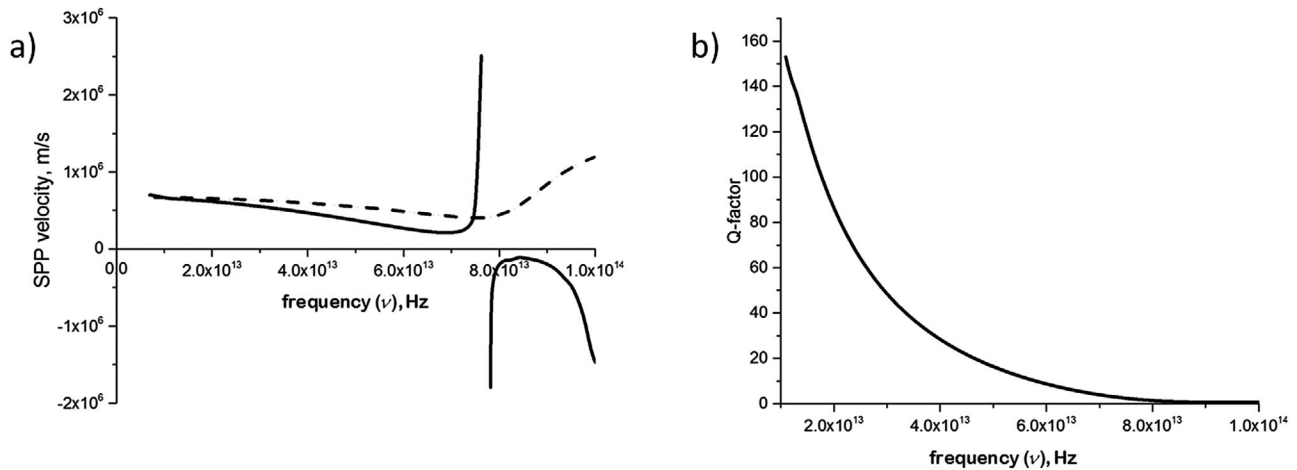
Figure 3. a) Group velocity (solid line) and phase velocity (dashed line) of SPP propagating in the DWCNT array for interlayer mode (Figure 2b, inset 3); b) Q-factor of interlayer mode in DWCNT (Figure 2b, inset 3).

at the frequencies up to 40–50 THz. Besides, due to the strong SPP confinement between layers in such modes the neighboring DWCNTs have almost no effect on each other. Thus, dense DWCNT arrays ensuring an effective conversion of the external pump energy into the SPP energy could be employed for design of slow-wave structures.

The devices based on the interaction between the SPP and drift current[15,36–39] exploit the electric field longitudinal component inherent to the interlayer modes. The parameter characterizing domination of the longitudinal field component[15]

$$\eta = \frac{|E_z|^2}{|E_x|^2 + |E_y|^2 + |E_z|^2} \tag{4}$$

ranges for interlayer modes from 0.85 to 0.65 within the frequency range of 20–60 THz allowing interaction of the SPP longitudinal field component with both a drift current in the configuration proposed elsewhere[15,36] and an electron beam.[40]

The group and phase velocities corresponding to the fundamental interlayer mode (Figure 2b, inset 3) are shown in **Figure 3**. Within the frequency range of 0–78 THz, the group velocity is a positive function of the frequency. Importantly, in the frequency range from 10 to 75 THz phase velocity is almost linear and changes from 7×10^5 m s^{-1} to 4×10^5 m s^{-1} thus providing an effective refractive index (the deceleration coefficient) lying within the range of 430–750. Such deceleration enables effective interaction of the SPP with the drift current running with the velocity of $0.5−1 \times 10^6$ m s^{-1} through the CNT,[41,42] i.e., the phase matching can be achieved. Thus, DWCNTs are promising for application in devices employing an interaction between the SPP and drift current. The theoretical formalism elaborated elsewhere[39,43] and our previous studies[15,36] can be used for this purpose.

4. Electron Beam Pumping

An excitation of SPP is a challenge in nanoplasmonics.[44,45] The use of the charged particle beams for pumping of the structure is

one of the SPP excitation method.[46–51] In contrast to the pumping by the drift current,[15,37] the electron beam pumping does not employ electrical contacts. In comparison with the optical pumping, this method avoids using the prisms or diffraction gratings introducing the light into the structure.[52,53]

A 3D model has been used to demonstrate plasmon excitation by an electron beam, schematic of the problem studied is shown in Figure 1. Boundary conditions along x and y directions are periodic (inset in Figure 1). The length of CNT in numerical simulation has been set to 1 µm (that is several wavelengths for the longest SPP wavelength in simulation), at the both ends of CNTs the perfectly matched layer (PML) boundary conditions has been used. Thus in fact, along z direction the CNT can be considered as infinite, and there are no reflections of SPP from its ends in our model.

An efficiency of SPP excitation by the electron beams is determined by the electron beam effective radius characterizing the distance the electron beam is still interacting with the SPP. This distance can be qualitatively estimated using the following consideration: a beam of electrons moving at the velocity v along the z axis is described by a current density[48,49]

$$\mathbf{J}(\mathbf{r}, t) = \hat{\mathbf{e}}_z \rho v \delta(x, y) \delta(z - vt) \tag{5}$$

where $\hat{\mathbf{e}}_z$ is the unit vector along z, ρ is the charge density, δ is the delta function. SPPs are excited by the electric field induced by the electron beam (5). The z-component of the electron beam field is assumed to decrease exponentially in the transverse direction as $e^{-k_\perp r}$, where r is cylindrical coordinate, $k_\perp$ is determined as[48]:

$$k_\perp = \omega \sqrt{\frac{1}{v_p^2} - \frac{1}{v^2}} \tag{6}$$

where v_p is the phase velocity of SPP interacting with an electron beam. At $v_p < v$, $k_\perp$ is a real value, i.e., the electric field of the

**ADVANCED
SCIENCE NEWS**

www.advancedsciencenews.com
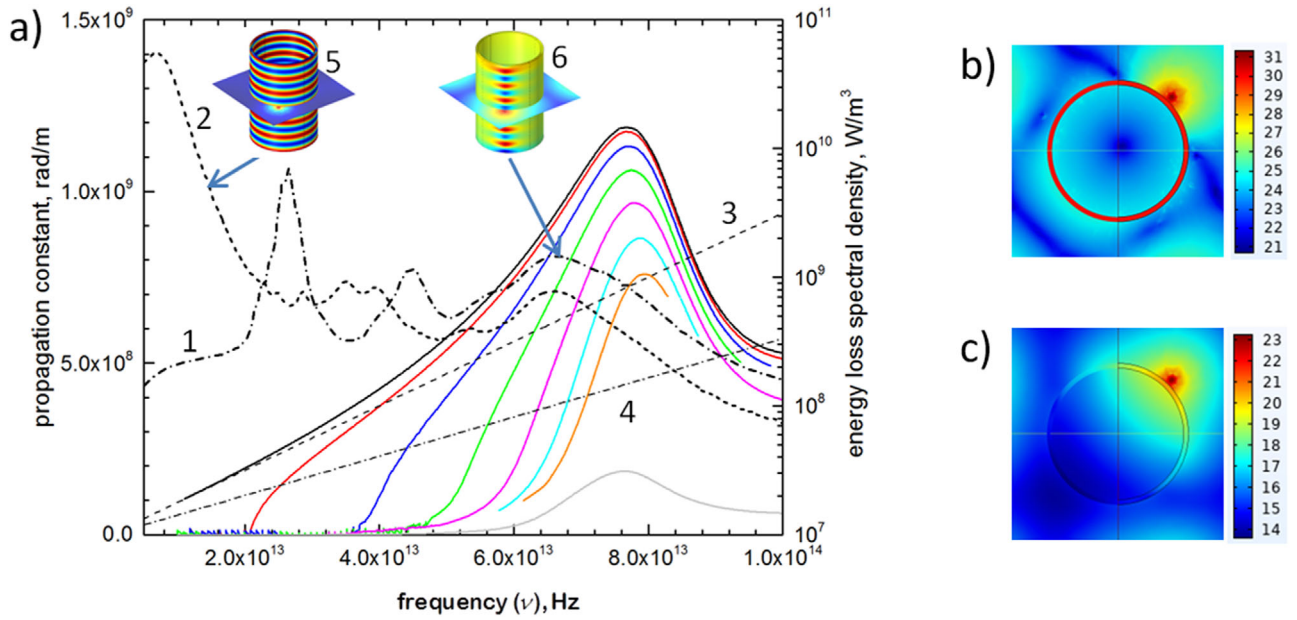
annalen
der **physik**

www.ann-phys.org

Figure 4. a) The SPP propagation constant (colored curves) and the spectral density of the electron energy losses (black curves) in DWCNT array. Curves (1) and (2) show the energy spectral density of electron beam losses (10). Straight lines (3) and (4) correspond to the current provided by electrons moving at velocities $v = 0.67 \times 10^6$ m s^{-1} and $v = 1.0 \times 10^6$ m s^{-1}, respectively. Insets (5) and (6) show the distribution of the z-component of electric field excited by an electron beam at frequencies of 15 and 65 THz, respectively. b,c) The electric field distribution (in a.u.) over the transverse cross-section of DWCNT at the frequencies of 15 THz (b) and 65 THz (c). The energy losses of the exciting SPP electron beam shown in Figure 4a are calculated per unit carbon nanotube (CNT) length.

electron beam decays exponentially in the transverse direction. So, the electron beam effective radius can be given as:

$$r_e \sim \frac{1}{k_\perp} = \frac{1}{\omega}\frac{v_p v}{\sqrt{v^2 - v_p^2}} \tag{7}$$

One can see that $r_e \to \infty$ at $v \to v_p$, i.e., when the velocities are matched. It means that the electrons moving at the velocity equal to the SPP phase velocity can effectively transfer energy to SPP. Since the velocity of free electrons v can be varied by tuning the accelerating voltage within a wide range, this solution simplifies the matching of the SPP and electron velocities in comparison with the drift current pumping[15,36,37] commonly used for this purpose.

The current (5) associated with the electron beam induces an electric field with the vector potential **A** determined by the expression:

$$\left(\nabla^2 + \varepsilon k_0^2\right)\mathbf{A}(\mathbf{r}, \omega) = -\mu_0 \mathbf{J}(\mathbf{r}, \omega) \tag{8}$$

where ε is relative permittivity of the medium. The SPP excitation efficiency can be estimated taking into account the energy loss of an electron moving along the nanotube[47,48]:

$$W_{EEL} = -\frac{1}{\pi}\int d\omega \; \mathrm{Re}\left[\mathbf{J}_1^*(\mathbf{r}, \omega) \cdot \mathbf{E}_z^{ind}(\mathbf{r}, \omega)\right] \tag{9}$$

where $\mathbf{J}_1(\mathbf{r}, \omega)$ is the Fourier component of the electron current (5), the relation

$$-\frac{1}{\pi}\mathrm{Re}\left[\mathbf{J}_1^*(\mathbf{r}, \omega) \cdot \mathbf{E}_z^{ind}(\mathbf{r}, \omega)\right] \tag{10}$$

is the spectral density of the electron energy losses,

$$\mathbf{J}_1(\mathbf{r}, \omega) = J_1(\mathbf{r}, \omega)\hat{\mathbf{e}}_z = \hat{\mathbf{e}}_z\left(\rho\delta(r_0)e^{i\frac{\omega}{v}z} + J'\right) = \hat{\mathbf{e}}_z\left(J_0 + J'\right) \tag{11}$$

$\mathbf{E}_z^{ind}(\mathbf{r}, \omega)$ is the electric field induced by the current $\mathbf{J}_1(\mathbf{r}, \omega)$ at the location of electron, r_0 is the distance from the CNT axis to the electron beam. Integration in (9) is performed over the whole frequency range ω. Expression (11) differs from the relation described elsewhere[48] by an additional term responsible for the SPP electric field feedback to the electron beam determined by the expression[17,18]:

$$\frac{\partial^2 J'}{\partial z^2} + 2i\beta_e\frac{\partial J'}{\partial z} - (\beta_e^2 - \beta_p^2)J' = i\frac{\beta_e J_0}{2V_0}E_z \tag{12}$$

where $\beta_e = \omega/v$, $\beta_p = \omega_p/v_p$, ω_p is the plasma frequency, V_0 is the voltage accelerating an electron beam.

5. Results and Discussion

The Fourier spectrum of electron beam energy losses (10) is shown in **Figure 4**a by lines (1) and (2). The straight lines (3) and (4) correspond to the current provided by electrons moving at different velocities ($v = 0.67 \times 10^6$ m s^{-1} and $v = 1.0 \times 10^6$ m s^{-1},

**ADVANCED
SCIENCE NEWS**

www.advancedsciencenews.com

annalen
der **physik**

www.ann-phys.org

respectively). Intersection points of the straight lines with the dispersion curves (colored lines in Figure 4a) are the phase matching points. Once the phase matching of SPP and electron beam is achieved, the SPP with the corresponding propagation constant is excited in a DWCNT. A high peak in the frequency range of 0–20 THz registered at the electron beam velocity $v = 0.67 \times 10^6$ m s^{-1} (Figure 4a line (2)) is the region where the phase matching is satisfied not only at one point but within the 0–20 THz frequency range due to vicinity of the SPP dispersion curve in this range to a straight line passing through the origin of coordinates. In this case, an azimuthally symmetric mode with low losses is excited in the CNT (Figure 4b), the peak height is determined by the high Q-factor (about 100 at low frequencies, see Figure 3b) of this mode described by expression (3).

Importantly, the calculated spectrum is complex and not completely determined by the phase matching condition. It is due to the fact that the electron beam excites not only the CNT eigenmodes described by dispersion relations (Figure 2). In our consideration, the electron beam exciting the SPP is always parallel to the CNT axis (Figure 1), whereas its position with respect to the CNT axis and walls could be different. Figure 4a–c (insets) illustrates a general case when the beam is outside the DWCNT and near its surface. One can see that when the CNT eigenmode is excited, the exciting field asymmetry does not affect the excited mode structure (Figure 4b). However, in the frequency range of 50–80 THz, one broad peak of energy loss spectral density almost independent of the electron beam velocity is observed for all electron beam velocities (Figure 4a) instead of many resonance peaks corresponding to the phase matching to the CNT eigenmodes. The nature of this broad maximum could be explained by the fact that the electron beam in the considered geometry excites an asymmetric wave not in the whole cross-section but only in some part of the CNT (Figure 4c), thus a wave is not a CNT eigenmode. Unlike the eigenmodes, this surface wave does not exhibit a resonant character of propagation in the azimuthal direction[54] resulting in appearance of a broad nonresonant maximum. In general, the high Q-factor resonant modes possess the highest intensities due to the positive feedback provided by the SPP excited by an electron beam to the electron beam (12), whereas the lower Q-factor eigenmodes are hidden by the nonresonant losses. Thus, most of the electron beam energy is pumped into the azimuthally symmetric mode with low losses (Figure 4b), whereas modes of the higher azimuthal order possess significantly lower Q-factor and cannot ensure such an efficient energy pumping.[36,54] The principal difference in behavior of the modes with different Q-factors is known in laser technology: lower Q-factor modes provide far weaker positive feedback.[55]

6. Conclusion

A simple model describing a DWCNT array has been proposed. It is shown that the high Q-factor highly confined SPP modes can exist in such arrays. Excitation of the surface plasmon modes by an electron beam has been investigated. The spectral density of electron beam energy transferred to the DWCNT modes is obtained by numerical calculations. We have determined the frequency range of SPP and electron beam velocities enabling the phase matching and efficient energy transfer within a wide frequency range. It has been shown that an efficient energy transfer

is provided by a linear part of the dispersion curve near the origin of coordinates. Thus, to satisfy the phase matching within a wide frequency range a proper electron velocity has to be provided in the experiment. All this contributes to elaboration of the slow-wave structures based on the dense arrays of double-walled CNTs enabling efficient conversion of the pump energy into the SPP energy.

Phase-matching simultaneously satisfied for a large array of parallel CNTs could be used for design of the IR- and THz generators based on the same operation principle as a traveling wave tube or the so-called O-type generators directly pumped by the injected or drift currents. In this case, the nonrelativistic electron beams with a speed less than 10^6 m s^{-1} could be employed for pumping. Since the interaction with the electron beam occurs over the entire area of the CNT array, the proposed slow-wave structrure is not limited in dimension in the transverse direction thus it allows scaling the pump currents and, hence, adjustment of the generated power.

Conflict of Interest

The authors declare no conflict of interest.

Data Availability Statement

The data that support the findings of this study are available from the corresponding author upon reasonable request.

[1] A. Heidari, in *Mobile Health* (Ed: S. Adibi), Springer, Berlin **2015**, pp. 663–670. https://doi.org/10.1007/978-3-319-12817-7_28.

[2] L. Yu, L. Hao, T. Meiqiong, H. Jiaoqi, L. Wei, D. Jinying, C. Xueping, F. Weiling, Z. Yang, *RSC Adv.* **2019**, *9*, 9354.

[3] A. Redo-Sanchez, B. Heshmat, A. Aghasi, S. Naqvi, M. Zhang, J. Romberg, R. Raskar, *Nat. Commun.* **2016**, *7*, 12665.

[4] W. Gao, C. F. Doiron, X. Li, J. Kono, G. V. Naik, *ACS Photonics* **2019**, *6*, 1602.

[5] J. A. Roberts, S. J. Yu, P. H. Ho, S. Schoeche, A. L. Falk, J. A. Fan, *Nano Lett.* **2019**, *19*, 3131.

[6] E. Lidorikis, A. C. Ferrari, *ACS Nano* **2009**, *3*, 1238.

[7] H. Butt, A. K. Yetisen, R. Ahmed, S. H. Yun, Q. Dai, *Appl. Phys. Lett.* **2015**, *106*, 121108.

[8] H. Bao, X. Ruan, T. S. Fisher, *Opt. Express* **2010**, *18*, 6347.

[9] S. M. Hashemi, I. S. Nefedov, *Phys. Rev. B: Condens. Matter Mater. Phys.* **2012**, *86*, 195411.

[10] X. L. Liu, R. Z. Zhang, Z. M. Zhang, *Appl. Phys. Lett.* **2013**, *103*, 213102.

[11] H. Butt, Q. Dai, P. Farah, T. Butler, T. D. Wilkinson, J. J. Baumberg, G. A. J. Amaratunga, *Appl. Phys. Lett.* **2010**, *97*, 2008.

[12] J. Hao, G. W. Hanson, *Phys. Rev. B: Condens. Matter Mater. Phys.* **2006**, *74*, 035119.

[13] Y. Wang, Z. Cui, X. Zhang, X. Zhang, Y. Zhu, S. Chen, H. Hu, *ACS Appl. Mater. Interfaces* **2020**, *12*, 52082.

[14] G. Y. Slepyan, S. a. Maksimenko, A. Lakhtakia, O. Yevtushenko, A. V. Gusakov, *Phys. Rev. B* **1999**, *60*, 17136.

[15] A. S. Kadochkin, S. G. Moiseev, Y. S. Dadoenkova, V. V. Svetukhin, I. O. Zolotovskii, *Opt. Express* **2017**, *25*, 27165.

[16] K. G. Batrakov, S. A. Maksimenko, P. P. Kuzhir, C. Thomsen, *Phys. Rev. B: Condens. Matter Mater. Phys.* **2009**, *79*, 125408.

[17] S. E. Tsimring, *Electron Beams and Microwave Vacuum Electronics*, John Wiley & Sons, Inc., Hoboken, NJ, USA **2006**. https://doi.org/10.1002/0470053763.

[18] D. I. Trubetskov, A. E. Khramov, *Lectures on Microwave Electronics for Physicists*, Fizmatlit, Moscow **2003**.

[19] F. R. G. Bagsican, M. Wais, N. Komatsu, W. Gao, L. W. Weber, K. Serita, H. Murakami, K. Held, F. A. Hegmann, M. Tonouchi, J. Kono, I. Kawayama, M. Battiato, *Nano Lett.* **2020**, *20*, 3098.

[20] W. Ruland, A. K. Schaper, H. Hou, A. Greiner, *Carbon* **2003**, *41*, 423.

[21] H. Furuta, T. Kawaharamura, M. Furuta, K. Kawabata, T. Hirao, T. Komukai, K. Yoshihara, Y. Shimomoto, T. Oguchi, *Appl. Phys. Express.* **2010**, *3*, 105101.

[22] Y. Ando, X. Zhao, H. Shimoyama, *Carbon* **2001**, *39*, 569.

[23] M. V. Shuba, G. Y. Slepyan, S. A. Maksimenko, C. Thomsen, A. Lakhtakia, *Phys. Rev. B: Condens. Matter Mater. Phys.* **2009**, *79*, 155403.

[24] R. Xiang, T. Inoue, Y. Zheng, A. Kumamoto, Y. Qian, Y. Sato, M. Liu, D. Tang, D. Gokhale, J. Guo, K. Hisama, S. Yotsumoto, T. Ogamoto, H. Arai, Y. Kobayashi, H. Zhang, B. Hou, A. Anisimov, M. Maruyama, Y. Miyata, S. Okada, S. Chiashi, Y. Li, J. Kong, E. I. Kauppinen, Y. Ikuhara, K. Suenaga, S. Maruyama, *Science* **2020**, *542*, 537.

[25] F. J. G. De Abajo, *ACS Photonics* **2014**, *1*, 135.

[26] B. Bourlon, C. Miko, L. Forró, D. C. Glattli, A. Bachtold, *Phys. Rev. Lett.* **2004**, *93*, 176806.

[27] Y. G. Yoon, P. Delaney, S. G. Louie, *Phys. Rev. B: Condens. Matter Mater. Phys.* **2002**, *66*, 734071.

[28] L. Martín-Moreno, F. J. G. De Abajo, F. J. García-Vidal, *Phys. Rev. Lett.* **2015**, *115*, 173601.

[29] P. Ayala, R. Arenal, M. Rümmeli, A. Rubio, T. Pichler, *Carbon* **2010**, *48*, 575.

[30] L. Duclaux, *Carbon* **2002**, *40*, 1751.

[31] L. A. Falkovsky, *Usp. Fiz. Nauk* **2008**, *178*, 923.

[32] L. A. Falkovsky, S. S. Pershoguba, *Phys. Rev. B: Condens. Matter Mater. Phys.* **2007**, *76*, 153410.

[33] P. Yu, V. I. Fesenko, V. R. Tuz, *Nanophotonics* **2018**, *7*, 925.

[34] A. Y. Nikitin, F. Guinea, F. J. García-Vidal, L. Martín-Moreno, *Phys. Rev. B: Condens. Matter Mater. Phys.* **2011**, *84*, 161407.

[35] Z. Wu, L. Wang, Y. Peng, A. Young, S. Seraphin, H. Xin, *J. Appl. Phys.* **2008**, *103*, 094324.

[36] A. S. Kadochkin, S. Moiseev, Y. S. Dadoenkova, F. Bentivegna, V. Svetukhin, I. O. Zolotovsky, *J. Opt.* **2020**, *22*, 125002.

[37] S. G. Moiseev, Y. S. Dadoenkova, A. S. Kadochkin, A. A. Fotiadi, V. V. Svetukhin, I. O. Zolotovskii, *Ann. Phys.* **2018**, *530*, 1800197.

[38] D. A. Svintsov, A. V. Arsenin, D. Y. Fedyanin, *Opt. Express* **2015**, *23*, 19358.

[39] T. A. Morgado, M. G. Silveirinha, *ACS Photonics* **2018**, *5*, 4253.

[40] D. Svintsov, *Phys. Rev. B* **2019**, *100*, 195428.

[41] V. Perebeinos, J. Tersoff, P. Avouris, *Phys. Rev. Lett.* **2005**, *94*, 2.

[42] K. Liu, J. Deslippe, F. Xiao, R. B. Capaz, X. Hong, S. Aloni, A. Zettl, W. Wang, X. Bai, S. G. Louie, E. Wang, F. Wang, *Nat. Nanotechnol.* **2012**, *7*, 325.

[43] T. A. Morgado, M. G. Silveirinha, *Phys. Rev. Lett.* **2017**, *119*, 133901.

[44] S. Wang, F. Wu, K. Watanabe, T. Taniguchi, C. Zhou, F. Wang, *Nano Lett.* **2020**, *20*, 2695.

[45] Z. Shi, X. Hong, H. A. Bechtel, B. Zeng, M. C. Martin, K. Watanabe, T. Taniguchi, Y. R. Shen, F. Wang, *Nat. Photonics* **2015**, *9*, 515.

[46] W. Cai, R. Sainidou, J. Xu, A. Polman, F. J. G. De Abajo, *Nano Lett.* **2009**, *9*, 1176.

[47] F. J. García De Abajo, *Rev. Mod. Phys.* **2010**, *82*, 209.

[48] T. Zhan, D. Han, X. Hu, X. Liu, S. T. Chui, J. Zi, *Phys. Rev. B: Condens. Matter Mater. Phys.* **2014**, *89*, 245434.

[49] S. Liu, P. Zhang, W. Liu, S. Gong, R. Zhong, Y. Zhang, M. Hu, *Phys. Rev. Lett.* **2012**, *109*, 153902.

[50] M. V. Bashevoy, F. Jonsson, A. V. Krasavin, N. I. Zheludev, Y. Chen, M. I. Stockman, *Nano Lett.* **2006**, *6*, 1113.

[51] F. J. García De Abajo, V. Di Giulio, *ACS Photonics.* **2021**, *8*, 945.

[52] B. E. Carlsten, *Phys. Plasmas* **2002**, *9*, 5088.

[53] Y. M. Shin, L. R. Barnett, N. C. Luhmann, *Appl. Phys. Lett.* **2008**, *93*, 221504.

[54] K. I. Sasaki, S. Murakami, H. Yamamoto, *Appl. Phys. Lett.* **2016**, *108*, 163109.

[55] A. Yariv, *Quantum Electronics*, Wiley, Weinheim **1989**.